Atomic contrast on ultrathin $La_{0.7}Sr_{0.3}MnO_3$ films by Scanning Tunnelling Microscopy

A. Gambardella,* P. Graziosi, I. Bergenti, M. Prezioso, F. Biscarini, V. Dediu

Consiglio Nazionale delle Ricerche - Istituto per lo Studio dei Materiali Nanostrutturati (CNR-ISMN), Bologna, Italy

Vincitore del Premio Carla Milanesi 2011

Corresponding author: Alessando Gambardella
Consiglio Nazionale delle Ricerche - Istituto per lo Studio dei Materiali Nanostrutturati (CNR-ISMN) via P. Gobetti 101, 40129 Bologna, Italy.
Tel. +39.051.639.85.17 - Fax +39.051.639.85.40
E-mail: a.gambardella@bo.ismn.cnr.it

Summary
In this work we map tunnel conductance curves and topographies with nanometric and sub-nanometric spatial resolution of fully insulating $La_{0.7}Sr_{0.3}MnO_3$ ultrathin films at room temperature. While spectroscopy shows the lack of spatial patterns, suggesting no strong correlation between topographic and spectroscopic features at room temperature, we obtained for the first time clear atomic contrast at only some surface locations. We justify our results by suggesting the presence of local intrinsic inhomogeneities, that would act on a surface with overall homogeneous electronic states as charge density reliever, by allowing atomic contrast by a tunnelling measurement. Furthermore, our findings suggest that the effect of strain is to induce a transition from weak- to strong-electron-phonon coupling regimes, making fully-strained films as interesting model-systems to investigate the nature of the electron correlation directly at nanoscale lengths.

Key words: manganites, STM, ultrathin films, highly correlated systems, atomic resolution.

Introduction

Perovskite manganites, having general formula $Re_{1-x}A_xMnO_3$ (where Re = Rare Earth, A = Divalent metal) have been often studied by Scanning Tunnelling Microscopy and Spectroscopy (STM-STS) techniques. Indeed, investigation of surface states with nanoscale resolution is strongly desirable on such highly-correlated systems, whose exotic properties arise from the coexistence of microscopic effects (Dagotto *et al.*, 2001). According to the definition given by Postorino (Postorino *et al.*, 2003) and based on the classification made by Millis (Millis *et al.*, 1996), perovskite manganites can be ordered according to three classes depending on the strength of the electron-phonon coupling. Manganites belonging to *weak* and *intermediate coupling* exhibit ferromagnetic (FM) to paramagnetic (PM) phase transition at the temperature T_c; above T_c the transport is believed to be governed by polarons due to strong phonon-electron coupling, mediated by Jahn-Teller distortion around the trivalent Mn^{3+} ion. Below T_c the ground state is metallic ($d\rho/dT>0$). The transition from the activated PM state to the metallic FM state is referred to as the Metal-Insulator-Transition (MIT). *Strong coupled* manganites do not exhibit MIT and are insulating over the whole range of temperature, although PM-FM transitions occur at temperatures depending on doping and/or composition. The study of the variation around the MIT of the density of states at the Fermi level $N_S(E_F)$ has constituted the main topic of investigation for many STM-STS experiments. Early works on thin films (Fath *et al.*, 1999; Becker *et al.*, 2002) were focused on the features of coexistence of carrier-rich FM metallic and carrier-deficient non-FM insulating regions up to the mesoscopic scale. Such phenomenon is known as electronic phase-separation (PS). The topographic contrast was used to distinguish between occupied and unoccupied states on epitaxial 120 nm thick film of $La_{5/8-0.3}Pr_{0.3}Ca_{5/8}MnO_3$ (Ma *et al.*, 2005) and $Bi_{0.24}Ca_{0.76}MnO_3$ single crystals (Renner *et al.*, 2002). Then, atomic contrast was proposed as marker for polaron confinement at the surface in layered rock-salt type manganites (RØnnow *et*

al., 2006; Bryat *et al.*, 2011), as well as in cubic $Pr_{0.68}Pb_{0.32}MnO_3$ (Rößler *et al.*, 2010). It is noteworthy that atomic contrast was obtained on manganese perovskite compounds belonging to the strong coupling class only, with the exception of the $Pr_{0.68}Pb_{0.32}MnO_3$ which comes from the intermediate coupling class. On the other hand, robust STS measurements on epitaxial $La_{0.7}Ca_{0.3}Mn_{O3}$ (LCMO) (Seiro *et al.*, 2010; Mitra *et al.*, 2005) or $La_{0.7}Sr_{0.3}MnO_3$ (LSMO) thin films (Singh *et al.*, 2008) found an homogeneous spectroscopic behaviour which suggested that no polarons are confined on both sides of the MIT (Seiro *et al.*, 2008). Nonetheless, scanning tunnelling experiments on such systems are useful to investigate the nature of the charge localization effect at the surface, still controversial to date. In bulky manganites, despite the low – if compared to metals – density of carriers ($\sim 10^{21}$ cm^{-3}), charge screening was indicated as a strong limiting factor on the maximum lateral resolution obtainable by STM (RØnnow *et al.*, 2006); anyway, by reviewing the works presented so far, it is not clear whether polarons, lattice inhomogeneities having a purely morphological origin, as well as intrinsic point defects, can be treated separately. Attempting to address these controversial aspects, we performed for the first time an extensive STM characterization on ultrathin manganite films. The striking difference between bulks and films arises from the film thickness; when it is reduced under a critical value (t_c), they show the lack of the MIT and fully-insulating behaviour regardless the temperature (Huijben *et al.*, 2008; Jin *et al.*, 2007). Surprisingly, scanning probe investigations on ultrathin manganite films (few unit cells thick) are rare (Rana *et al.*, 2010), despite of the interest into ultrathin epitaxial films (2D) where small changes in structure or composition affect significantly the electronic structure and therefore the macroscopic properties (Huijben *et al.*, 2008; Bergenti *et al.*, 2007). Transport and and magneto-optical measurements performed on ultrathin manganite films (Aruta *et al.*, 2009; Orgiani *et al.*, 2007) have remarked the role played by chemical or structural inhomogeneities, such as point defects and/or intrinsic lattice deformations. In this topic, fully-strained manganite films represent an interesting model-system for high-resolution STM analysis either for the electronic contrast mechanism or the direct investigation of inhomogeneities, since charge screening is expected to be naturally reduced *a priori* by the poor surface conductivity, similarly to what happens in semiconductors where resolution of individual atoms is related to the presence of localized electronic states on the surface around E_F, which contribute as local variations in the probing tunnel current.

Materials and Methods

Here we present an STM characterization of two doped $La_{0.7}Sr_{0.3}MnO_3$ (LSMO) films -5 and -9 unit cells thick, respectively deposited on cubic (a = 3.90Å) $SrTiO_3$ (STO) substrates. This compound shows Colossal Magneto Resistance (CMR) effect at high temperatures and was successfully employed in the form of epitaxial films in the fabrication of spin-transport-based devices (Preziosi *et al.*, 2011; Barraud *et al.*, 2010). LSMO films were grown by Channel Spark Ablation technique, already used to produce epitaxial films as described elsewhere (Bergenti *et al.*, 2007; Dediu *et al.*, 1999). Film thicknesses were evaluated by X-Ray Reflectivity (XRR) measurements. Bulk $La_{0.7}Sr_{0.3}MnO_3$ is rhombohedral at room temperature, having pseudocubic parameter a=3.873Å and a distorted pseudocubic angle α= 90.26°(Trukhanov *et al.*, 2007). The STM-STS measurements were carried out at 298K and Ultra High Vacuum (UHV) conditions by using a commercial instrument. After being transferred into UHV chamber, samples were heated in-situ at 120°C for a few hours, and successively left to cool for many hours before the measurements. Cut PtIr wires tips were used and the surfaces imaged mainly in the topographic mode with an applied tip-biased voltage of ~1V. Setpoint current of 100-120 pA was required to achieve atomic contrast on both samples. The measurement parameters were adjusted repeatedly in order to reduce artefacts due to the scan operation and thermal drift distortion. DC Transport measurements were performed by a cryogenic apparatus with four-probe method. As shown in Figure 1d, our ultrathin films experience the lack of the MIT as expected for fully strained samples, on the whole temperature range. Despite of the high spatial resolution (up to 1 nm^2), the strong reproducibility and the good (40 meV) energy resolution of STS measurements, our I(V) curves should be taken an indication of the surface spec-

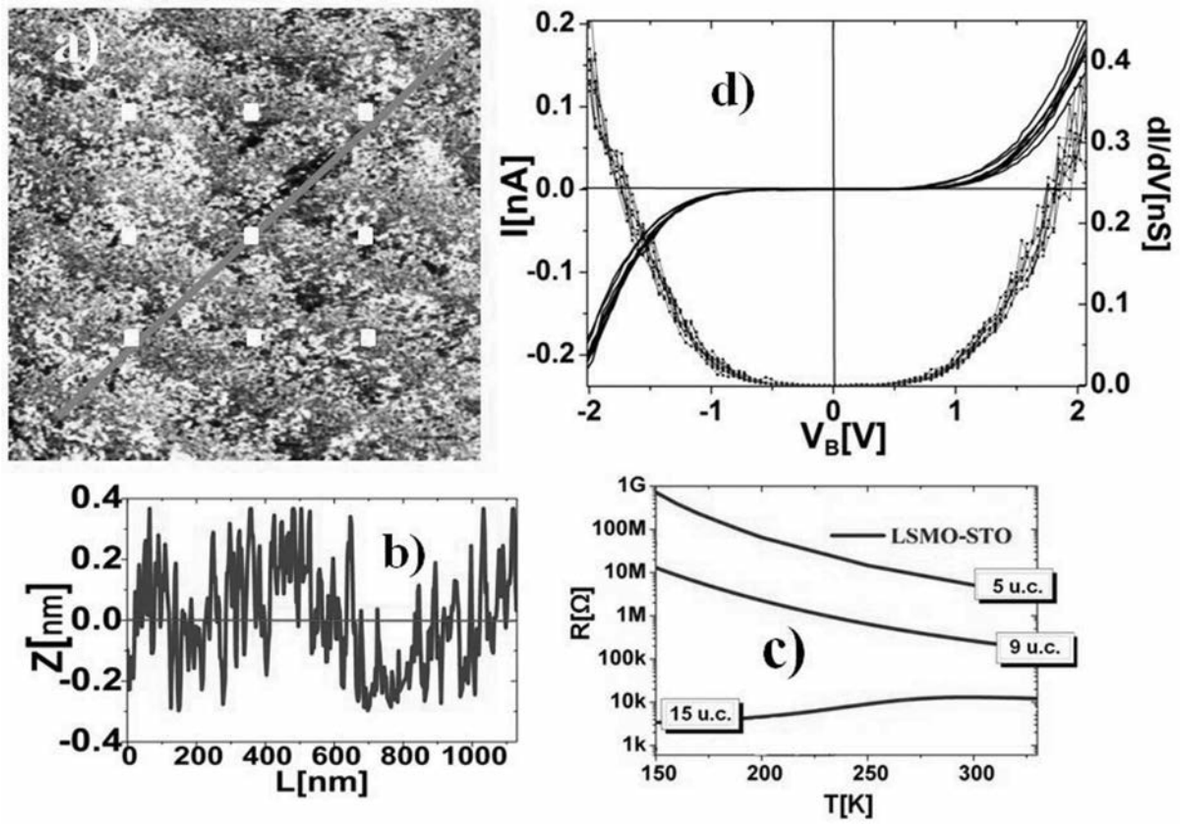

Figure 1. a) Constant current image of a 1 x 1 µ2 region taken on a 5 u.c. thick sample showing a largely terraced surface. b) Z-profile taken along the blue path on image a), showing that peak-to-peak roughness variations are within ± 1 u.c. (~ 0.4 nm). c) Resistance *vs* Temperature curves plotted for three different film of thicknesses, showing the lack of the MIT when thickness is under 6 nm, as samples under our investigation. d) Bare I(V) and corresponding dI/dV characteristics recorded over the surface in a) at RT; each curve is obtained by an average of 36 curves recorded within a single 60 x 60 nm2 large region, (the spectroscopy spatial resolution being 10×10 nm^2/spectrum), at the locations labelled by squares on image a). Topography and I(V) curves were measured at regulation conditions of 1V and 0.1 nA.

troscopy, rather than a direct estimation of the local Density of States (DOS). It is known that the tunnelling relation

$$\frac{dI}{dV} \approx \frac{e^2}{\hbar^2} \rho_S(eV)\rho_T(0)T(e,V,z),$$

where ρ_s (eV) is the sample DOS, ρ_t (0) is the tip DOS and $T(e,V,z)$ is the tunnelling coefficient within the barrier, is valid at low ($eV<<\phi$) biases, with ϕ= work function, whereas $T(e,V,z)$ does not depends on the energy (Tersoff and Hamann 1983). Moreover, it should be noted that curve representation as logarithmic derivative dlnI/dlnV would be more appropriate in this case (Stroscio *et al.*), but it requires higher energy resolution, which is normally associated to criogenic measurements.

Results

A typical topography showing a 1×1 µm^2 large sample region is presented in Fig. 1a. It reveals growth terraces roughly 100-200 nm wide, having steps of height about 1 unit cell (Figure 1b). Moreover we observed the absence of outgrowth up to 5×5 µm^2 large areas. Note that on these scales it

is not possible to indicate a unique terminating plane in the whole surface. The measurements show the Root Mean Square (RMS) roughness on both 5 and 9 u.c. thick samples being about one half of unit cell (~ 0.2 nm). Figure 1d shows the averaged tunnelling spectroscopy curves performed at 9 positions above the surface; curves were acquired simultaneously with imaging, and the exact locations are shown in the topographic image in a). Even near to terrace steps, local I(V) curves show the lack of spatial patterns in the energy range investigated, suggesting no strong correlation between topographic and spectroscopic features at room temperature. The surface is constituted by grains having a slightly mounded shape, 10-20 nm wide and a few cells high, as shown in Figure 2a, whose presence was already recognized among manganites grown by Pulsed Laser Deposition technique (Seiro *et al.*, 2008). Note that the dimensions of these mounds tend to slightly increase with the film thickness, although we observed no significant changes of morphology from the insulating toward the semi-metallic thickness regime (Singh *et al.*, 2008). Figure 2 shows the averaged I(V) and dI/dV curves taken on a 30×30 nm^2 regions, where mounds are clearly visible. Note that the increased spatial resolution reveals some differences between the curves acquired among different image locations, especially for negative biases. This discrepancies were observed before on a 5 nm thick LSMO film on larger scales, and ascribed to local stress of topographic steps that distort the lattice and disperse the electronic states (Rana *et al.*, 2010). We obtained clear atomic contrast at room temperature on both 5 and 9 u.c. thick samples, by visualizing the unit cell, as shown in the Figures 3 and 4. Nevertheless, we observed that the atomic contrast is limited to only few small (a few square nanometers) regions upon the samples surface.

Discussion and Conclusions

Among the scales investigated in this work, previous reports have already shown the absence of nanoscale modulation around the MIT on LSMO (Singh *et al.*, 2008; Seiro *et al.*, 2007; Seiro *et al.*, 2008) or only small variations (Rana *et al.*, 2010). The absence of an extrinsic phase separation lead to consider the spatial average of I(V) curves as representative of the whole sample surface. Findings of atomic contrast in Figure 3a,b and c, related to the 5 cell thick sample seems to suggest that a localised impurity or defect whose field locally may relieve the charge screening upon a length of some or tens of nm allows atomic resolution on such a region. This picture is supported

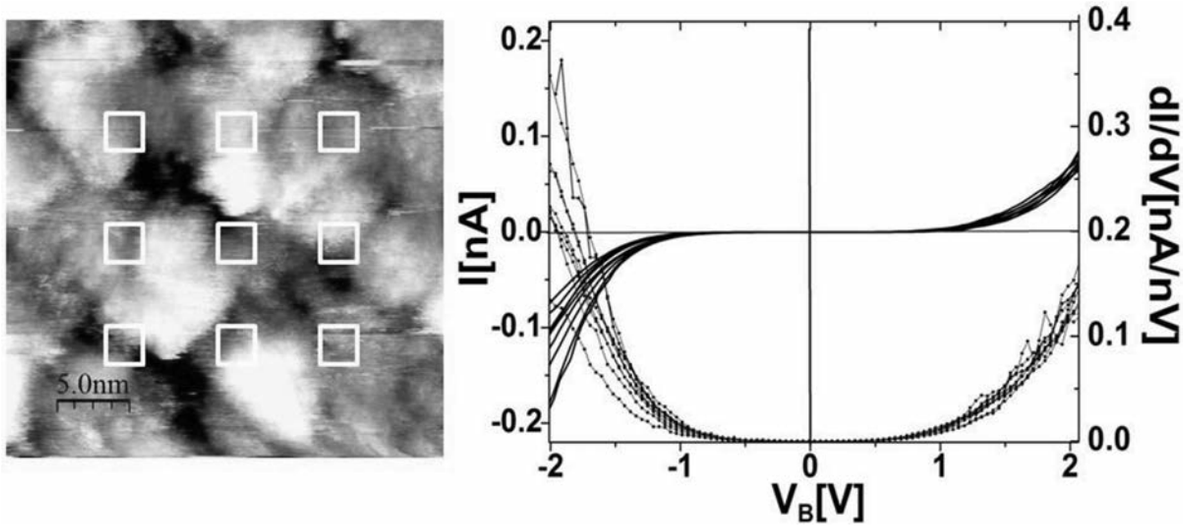

Figure 2. Averaged I(V) and corresponding dI/dV curves taken on the region 30 × 30 nm^2 in the inset at the 9 indicated positions. This region was taken within the region in Figure 1a. The surface granular structure is clearly visible but no direct evidence of correlation between spectra and topographic features is found, although spectra show quite different behaviour at negative biases.

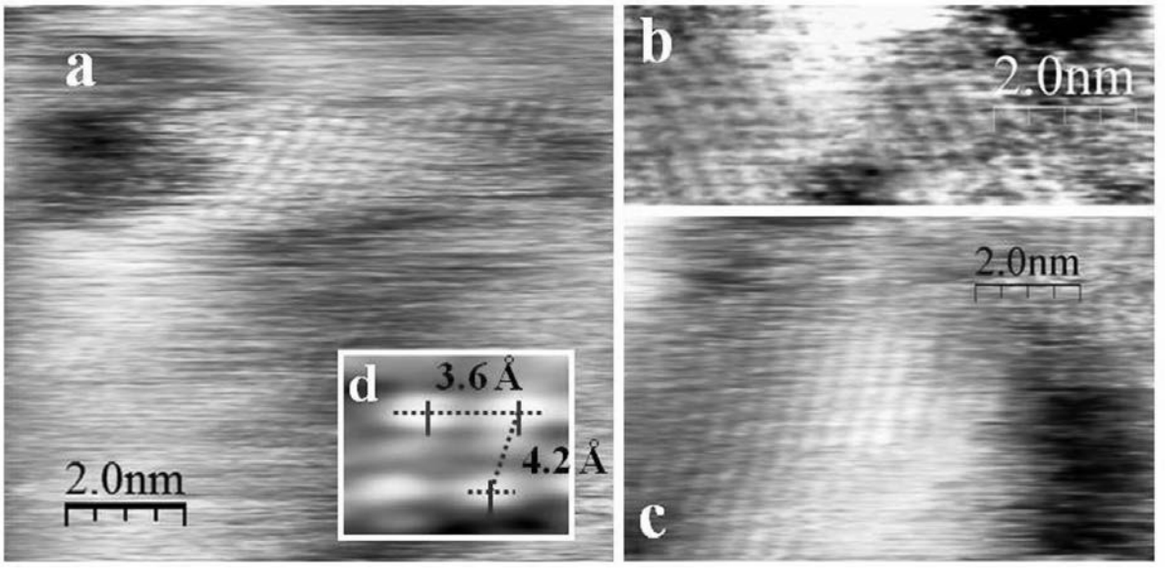

Figure 3. a), b), c), d) Atomically resolved images on a 5 cells-thick LSMO/STO sample. Different orientations of the atomic layers are found on three different regions located at about 5-10 nm of distance each others. Note the presence of defects (more darker or brighter regions) having maximum step heights of about 0.4 nm. In d) an image of a typical unit cell having distorted shape is shown, taken on a fourth region (not reported here entirely). Topographies were recorded at V_{bias} = 1.2V, I =120 pA.

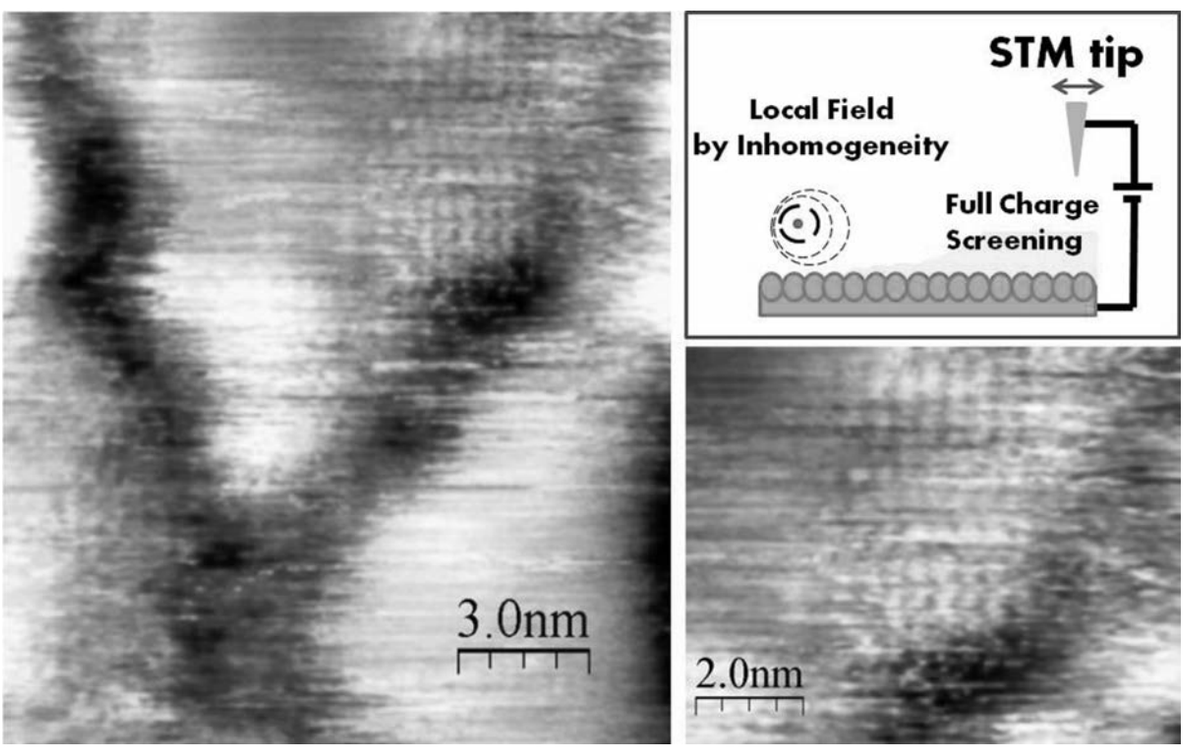

Figure 4. a) 12×12 nm^2 topography over the 9 u.c. thick sample. Atomic contrast is more clearly visible near to the terraces boundaries and over more internal regions located close to "huge" defects as in b) were a detail of a) is shown. c) The proposed mechanism for the charge relieving.

by our findings on the 9 cell thick sample, and shown in Figure 4, on a 13×13 nm^2 area. Atomic contrast is obtained especially close to topographic steps or mounds boundary, -the latter is expected to be a source of mismatch defects-, that may act as local scattering centres and locally favour the atomic resolution, even on an atomically flat surface and in presence of quite *homogeneous surface conduction*, as supported by our I(V) characteristics. We therefore suggest that surface inhomogeneities may locally increase the charge localization, by allowing or participating to the atomic contrast in a tunnelling measurements. One may infer that among bulks, inhomogeneities act *ipso facto* as the counterpart of the metallicity in surface state localization. As a further consideration, we often observed a strongly distorted cell, as clearly visible from the Figure 3 and 4, whose interatomic distances appear often quite different with respect to the picture of a square cell, as commonly assumed in literature. These distortions are evident in some regions on the 5 u.c. thick sample, and seem to be linked to local surface features rather than to scan/thermal drift effects, that are controlled to any possible extent. Cell distortions might be explained by the presence of intrinsic Moiré patterns, due to a interference coupling between the topmost and the inner atomic layer. It is clear that this occurrence would indicates by itself the presence of lattice discontinuities; however, this hypothesis is hardly justifiable due to the unclearness of the relieving mechanism, especially out-of-plane. Otherwise, we observed that the growth mode favours at the top layer the formation on non-uniform and atomically-stepped regions where, the surface reconstruction is not complete. In other words, the film growth appears epitaxial and coherent unless the last few atomic layer near the surface, making the presence of local defects related only to surface reconstruction. It is possible that these defects may act as scattering centres for the charge relieving, in the sense described above, and occasionally cause local strong lattice distortions as those shown in Figure 3. In reason of this, we suggest that the observed cell distortions are originated by an incomplete surface reconstruction. In conclusion, it is remarkable that bulk LSMO belongs to the weak coupling class, i.e. a family of manganese perovskite where people never succeeded in obtaining STM atomic resolution. We are able to affirm, thus, that the substrate-induced strain induces a so higher *e-ph* coupling that the materials is thrown in another class of manganese perovskite compounds, the strong coupling one (or phase segregated), which does not feature MIT and allowed for STM atomic contrast for the reasons discussed previously. Fully strained manganite thin films reveal to be an excellent tool to manipulate the physical state of the manganese perovskites playing with *e-ph* coupling and MIT, offering optimal candidates for basic solid state physics. In our experience, no surface preparation was required to achieve these results that were obtained at basic environmental and experimental conditions.

Acknoledgements

The authors would thank S. Milita for X-Ray Reflectivity measurements, performed at the Institute for Microelectronic and Microsystems, IMM-CNR. This work was supported by the project NMP-2009-246102 (IFOX).

References

Aruta C, Ghiringhelli G, Bisogni V, Braicovich L, Brookes N B, Tebano A et al. Orbital occupation, atomic moments, and magnetic ordering at interfaces of manganite thin films. Phys Rev B 2009;80:014431-39.

Barraud C, Seneor P, Mattana R, Fusil S, Bouzehouane K, Deranlot C, et al. Unravelling the role of the interface for spin injection into organic semiconductors. Nat Phys 2010;6:615-20.

Becker T, Streng C, Luo Y, Moshnyaga V, Damaschke B, Shannon N et al. Intrinsic Inhomogeneities in Manganite Thin Films Investigated with Scanning Tunneling Spectroscopy. Phys Rev Lett 2002;89:237203-7.

Bergenti I, Riminucci A, Arisi E, Hueso L. E, Cavallini M, Solzi M, et al. Ultrathin manganite films grown by pulsed-plasma deposition. J Magn Magn Mater 2007;310:e780–2.

Bryant B, Renner Ch, Tokunaga Y, Tokura Y, Aeppli G. Imaging oxygen defects and their motion at a manganite surface. Nat Commun 2011;2:212.

Dagotto E, T. Hotta T, A. Moreo A. Colossal Magnetoresistant Materials: The Key Role of Phase

Separation. Phys Rep 2001;344:1-153.
Dediu V, Lopez J, Matacotta F C, Nozar P, Ruani G, Zamboni R. Micro-Raman and Resistance Measurements of Epitaxial La0.7Sr0.3MnO3 Films. Phys Status Solidi B 1999;215:625-9.
Fath M, Friesem S. Menovsky A A, Tomioka Y, Aarts J, Mydosh J. Spatially Inhomogeneous Metal-Insulator Transition in Doped Manganites. Science 1999;285:1540-2.
Huijben M, Martin L W, Chu Y-H, Holcomb M B, Yu P, Rijnders G et al. Critical thickness and orbital ordering in ultrathin La0.7Sr0.3MnO3films. Phys Rev B 2008;78:094413-20.
Jin S, Gao G, Wu W, Zhou X. Effect of angular-distortion-induced strain on structural and transport properties of epitaxial La0.7Sr0.3MnO3 thin films. J. Phys. D 2007;40:305–9
Ma J X, Gillaspie D T, Plummer W, Shen J. Visualization of Localized Holes in Manganite Thin Films with Atomic Resolution. Phys Rev Lett 2005;95:237210-4.
Millis A J, Mueller R, Shraiman B I. Fermi-liquid-to-polaron crossover. II. Double exchange and the physics of colossal magnetoresistance. Phys. Rev. B 1996;54:5405–17.
Mitra J, Paranjape M, Raychaudhuri A K, Mathur N D, Blamire M G. Temperature dependence of density of states near the Fermi level in a strain-free epitaxial film of the hole-doped manganite La0.7Ca0.3MnO3. Phys Rev B 2005;71:094426-34.
Orgiani P, Adamo C, Barone C, Galdi A, Petrov A, Schlom et al. Influence of a single disorder parameter on the conduction mechanisms in manganite thin films. Phys Rev B 2007;76:012404-8.
Preziosi M, Riminucci A, Bergenti I, Graziosi P, Brunel D, Dediu V. Electrically Programmable Magnetoresistance in Multifunctional Organic-Based Spin Valve Devices. Adv Mater 2011;23:1371-5.
Postorino P, Congeduti A, Dore P, Sacchetti A, Gorelli F, Ulivi L, et al. Pressure Tuning of Electron-Phonon Coupling: The Insulator to Metal Transition in Manganites. Phys Rev Lett 2003;91:175501-5.
Rana A, Bogle K, Game O, Patil S, Valanoor N, Ogale S. Nanoscale modulation of electronic states across unit cell steps on the surface of an epitaxial colossal magnetoresistance manganite film. Appl Phys Lett 2010;96:263108-11.
Rößler S, Padmanabhan B, Elizabeth S, Bhat H L, Steglich F, Wirth S. Atomically resolved scanning tunneling microscopy on perovskite manganite single crystals. Appl Phys Lett 2010;96:202512-5.
Rong Z Y, Kuiper P. Electronic effects in scanning tunneling microscopy: Moiré pattern on a graphite surface. Phys. Rev. B 1993;48:17427–31.
RØnnow H M, Renner, Aeppli Ch G, Kimura T, Tokura Y. Polarons and confinement of electronic motion to two dimensions in a layered manganite. Nature (London) 2006;440:1025-8.
Seiro S, Fasano Y, Maggio-Aprile I, Kuffer O, Fischer Ø. Homogeneous spectroscopic properties in manganite films. J Magn Magn Mater 2007;310:e243-5.
Seiro S, Fasano Y, Maggio-Aprile I, Koller E, Kuffer O, Fischer Ø. Polaronic signature in the metallic phase of La0.7Ca0.3MnO3 films detected by scanning tunneling spectroscopy. Phys Rev B 2008;77:020407(R)1-4.
Singh U R, Gupta A K, Sheet G, Chandrasekhar V, Jang H W, Eom C B. Pseudogap formation in the metallic state of La0.7Sr0.3MnO3 thin films. Appl Phys Lett 2008;93:212503-6
Stroscio A J, Feenstra R M, Fein A. Electronic Structure of the Si(111)2 × 1 Surface by Scanning Tunneling Microscopy. Phys. Rev. Lett. 1986;57:2579-82
Tersoff J, Hamann D R. Theory and Application for the Scanning Tunneling Microscope. Phys. Rev. Lett. 1983;50:1998-2001
Trukhanov S V, Troyanchuk I O, Bobrikov I A, Simkin V G, Balagurov A M. Crystal structure phase separation in anion-deficient La0.70Sr0.30MnO3 – δ manganite system. J Surf Invest X-Ray+ 2007;1:6